Dynamics of turbulent transport in the scrape-off layer of the CASTOR tokamak

P. Devynck
Association EURATOM-CEA, CEA/DSM/DRFC Cadarache, 13108 Saint Paul Lez Durance, France

J. Brotankova
Institute of Plasma Physics, Association EURATOM-IPP.CR, Prague, Czech Republic

P. Peleman
Department of Applied Physics, Ghent University, Ghent, Belgium

M. Spolaore
Consorzio RFX, Associazione EURATOM-ENEA sulla Fusione, Padova, Italy

H. Figueiredo
Association EURATOM/IST, Lisbon, Portugal

M. Hron
Institute of Plasma Physics, Association EURATOM-IPP.CR, Prague, Czech Republic

G. Kirnev
Nuclear Fusion Institute, Kurchatov Institute, Moscow, Russia

E. Martines
Consorzio RFX, Associazione EURATOM-ENEA sulla Fusione, Padova, Italy

J. Stockel
Institute of Plasma Physics, Association EURATOM-IPP.CR, Prague, Czech Republic

G. Van Oost
Department of Applied Physics, Ghent University, Ghent, Belgium

V. Weinzettl
Institute of Plasma Physics, Association EURATOM-IPP.CR, Prague, Czech Republic

(Received 25 August 2006; accepted 13 September 2006; published online 16 October 2006)

In this paper, the propagation of turbulent events along radial and poloidal probe arrays in the scrape-off layer (SOL) of the tokamak CASTOR [M. Hron *et al.*, Czech. J. Phys. **49**, 181 (1999)] is observed using a novel correlation technique. The typical turbulent structures appear as dipoles on the floating potential signals and as positive bursts on the density. It is found that both dipoles and density bursts propagate over long radial distances in the SOL while propagating poloidally. A comparison of the measured velocities of the potential and density fluctuations shows that the density structures move radially faster than the potential ones. This allows us to understand how the density is convected by the turbulence. The density moves radially along the potential valleys created by the poloidal dipoles without modifying them. In the framework of an interchange turbulence, this property indicates that charge exchange collisions with neutrals in the SOL of CASTOR lead to a high viscosity that damps the zonal flows. © *2006 American Institute of Physics*. [DOI: 10.1063/1.2359721]

I. INTRODUCTION

The turbulence in the scrape-off layer (SOL) of fusion devices has been studied intensively over the past few years with the goal of understanding how the transport of matter and energy occurs in this region. The picture of the transport that was supposed to be diffusive at the beginning of the 1980s has evolved toward a convective type of transport. In particular, large and fast density bursts are believed to play a key role in the transport process. They are observed to travel in the SOL over long radial distances with typical radial velocities equal to a fraction of the ion sound speed. Such events are not dangerous in present-day machines, but they may become a nuisance in large devices such as ITER [Fusion Engineering and Design, 55 (2-3) 2001], where they may cause unacceptable heat load of the first wall and transport of tritium to unwanted portions of the wall structures.

These bursts have been observed with Langmuir probes[1–4] and recently their radial propagation has been observed with fast charge-coupled device (CCD) cameras over a few mm.[5,6] However, in the case of cameras, at the moment there is a lack of statistics and it is not clear if the events observed by the cameras are systematic or have a sufficient repetition rate to really characterize the transport. Also the limited dynamics of the existing cameras does not allow to follow a burst penetration very deep in the SOL where the light emission is scarce. In this paper, we use arrays of Lang-

muir probes to study the radial propagation of selected turbulent events over a distance of 3 cm. We define typical events both for floating potential and density fluctuations and follow their propagation along the probe array to gain some insight about the cross field transport process and the state of the turbulence. We compare the measured velocities of both the density and potential to understand how the bursts propagate in CASTOR, and this also gives information about the state of the turbulence and the edge conditions for CASTOR.

II. EXPERIMENTAL SETUP

The CASTOR tokamak ($R=0.4$ m, $a=0.085$ m) is operated at $Bt=1.3$ T, $Ip=12$ kA, and at the mean average density $ne=1\times10^{19}$ m^{-3}. The duration of the quasistationary phase of the discharge is 20 ms. During the shots presented here, a graphite electrode is inserted from the top of the torus and biased positively. However, we discuss exclusively the ohmic phase at the end of the discharge ($17<t<21$ ms). The biasing phase of the discharge has been discussed in Refs. 7–9. A so-called rake probe, made of 16 tips radially separated by 2.5 mm, is inserted from the top of the machine at an other toroidal location. The radial profiles of floating potential (V_f) or ion saturation current (I_{sat}) are measured in a single shot over the 16 tips with a sampling frequency of 1 MHz. During the time window of the analysis ($17<t<21$ ms), most of the tips appear to be inside the SOL due to a downward shift of the plasma column.

Another series of shots is also analyzed in this work with a different experimental setup. A poloidal ring of Langmuir tips covering the whole perimeter and radially positioned at $r=60$ mm is used to measure simultaneously the poloidal velocity of potential and density fluctuations. Two adjacent tips are separated by 3 mm and one tip out of two measures the ion saturation current I_{sat}. In these shots, the plasma current is adjusted so that the safety factor at the edge is $q(a)=8$. Due to the poloidal ring, the minor radius is reduced to $a=60$ mm. Because of a vertical shift of the plasma column, two quadrants of the ring are located inside the SOL. In each shot only data from one quadrant, corresponding to 32 tips (16 in I_{sat}, 16 in floating potential), are acquired with a sampling frequency of 1 MHz.

III. DATA ANALYSIS

The goal of the analysis is to observe the propagation of selected events along the rake probe as a function of time: This will in principle allow the observation of single trajectories and will give information about the transport processes driven by the turbulence. However, one of the difficulties is that in general, a specified type of event will propagate on the probes but will also change shape during its propagation. To overcome this problem, we use a correlation technique. At first, we select a subset $E(t)$ from the whole time series $S(t)$ that is believed to be a typical event. This event has a characteristic shape and a given duration $\tau=M\Delta t$, where Δt is the sampling interval. Both the shape and duration of the event can be deduced from the autocorrelation function of the signal.

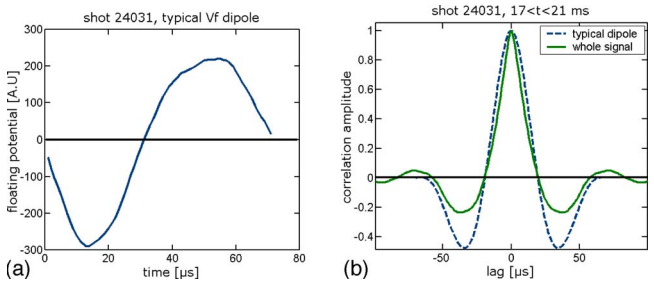

FIG. 1. (Left) Typical potential dipole measured on a probe of the rake located in the SOL. Such a structure is a characteristic one also encountered on the other probes. Reference signal E1. (Right) Comparison of autocorrelation function of typical dipole E1 with autocorrelation function of the whole signal.

After selecting the event, we define a specific correlation function,

$$C(t_j)=\frac{\sum_{i=1}^{M} S(t_j+i\Delta t)E(i\Delta t)}{\sqrt{\sum_{i=1}^{M} S(t_j+i\Delta t)^2\sum_{i=1}^{M} E(i\Delta t)^2}}. \quad (1)$$

The result of the procedure is a correlation function $C(t)$, which indicates how the data compare to the event E as a function of time. $C(t)$ can only take values between -1 and $+1$ [1 meaning that the signal of the time window starting at t_j and of duration τ is equal to E, -1 meaning same shape but opposite sign]. In order to keep only the events similar to E, all the values of $C(t)$ below a certain threshold (for example, 0.6) are set to 0. This procedure is repeated for all the tips of the rake probe, keeping the selected event E unchanged.

IV. POTENTIAL FLUCTUATIONS:

A. Typical structures: Potential dipoles

It has been observed in a previous article[10] that the potential fluctuations have a dipolar character in the SOL of CASTOR and rotate poloidally with a velocity compatible with the $E_r\times B_t$ plasma velocity. The dipolar character observed in different machines[11–14] has consequences on the skewness of the potential fluctuations, which is generally found to be reduced compared to that of the density fluctuations. We find, however, that this is not the case in CASTOR, as will be discussed later. Figure 1(a) shows a dipolar structure selected on one of the tips close to the last closed flux surface (LCFS), which is labeled E1 further in the text.

On the rake probe, this typical structure has a duration of about 70 μs and in general the negative peak is larger than the positive one. This shape is observed in the time domain, but if this structure is frozen in time during its poloidal propagation, the dipolar structure in time translates into a dipole in space, which is oriented in the poloidal direction. Consequently, this poloidal dipole creates a strong poloidal

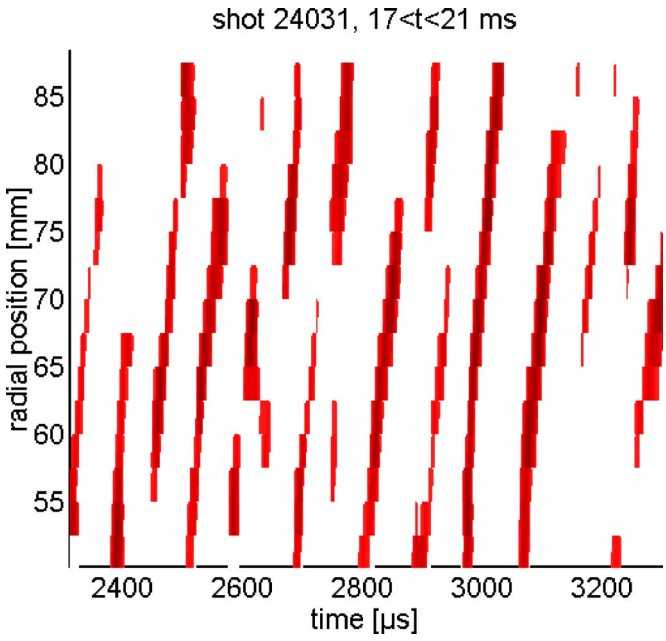

FIG. 2. Trajectories of dipoles type E1, along the rake probe in the SOL of CASTOR.

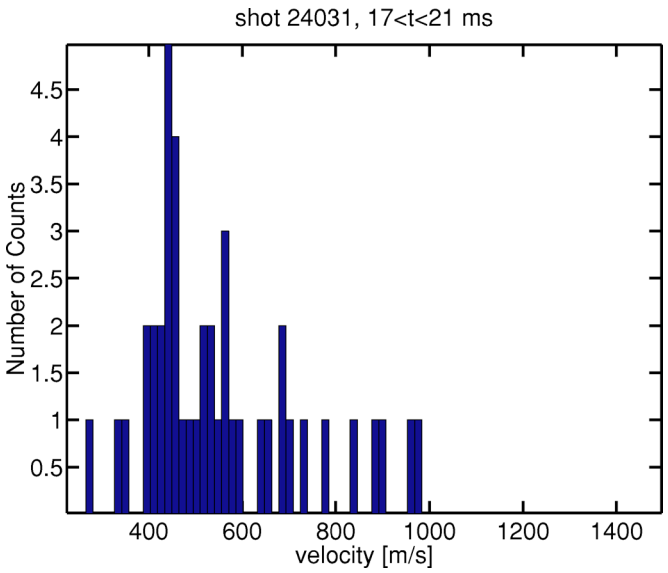

FIG. 3. Histogram of apparent radial velocities of dipoles type E1 on the rake.

electric field δE_θ, which in turn causes a radial drift velocity $\delta v_r = \delta E_\theta \times B_t / B_t^2$. Figure 1(b) allows us to compare the autocorrelation function (ACF) of the floating potential fluctuations with that of E1. The existence of an oscillation on the autocorrelation function of the Vf fluctuations indicates the presence of coherent dipoles in the signal. Figure 1(b) shows that E1 is correctly chosen as it reproduces the time scale of the Vf oscillating correlation function.

It must be noted that the event E1 displayed in Fig. 1(a) (first negative then positive) gives a radial velocity toward the wall. However, opposite dipoles (first positive then negative) that give a radial velocity oriented toward the plasma core are also found to exist in a similar amount.

B. Trajectories of the dipoles on the rake in the SOL

We focus here on data measured in the time window $17 < t < 21$ ms. As stated above, during this time window, the plasma is shifted downward and 12 of the 16 probes are now located inside the SOL. Figure 2 shows the trajectories of dipoles of type E1, which have correlation $C(t) > 0.6$. The trajectories of these dipoles are found to be radially elongated and inclined. Since they are well separated from one another, it is possible to follow the motion of each of them along the rake probe. First of all, the angle in the plane of Fig. 3 allows us to calculate the apparent radial velocity. A histogram of the velocities of the dipoles that extend at least over four consecutive probes is plotted in Fig. 3. The mean value is $\langle v_{\text{dipole}} \rangle = 580$ m/s while the most probable value is about 450 m/s. The standard deviation is $\sigma(v_{\text{dipole}}) = 250$ m/s. As stated above, the radial velocities of the dipoles plotted in Fig. 3 are only apparent and must not be interpreted in a straightforward way. References 11 and 12 show that the potential dipoles are inclined structures in the (r, θ) plane moving poloidally with a velocity comparable to the $E_r \times B_t$ one. Therefore, the radial propagation seen in Figs. 2 and 3 may be only a result of the projection of this poloidal motion on the rake probe.

As far as the radial extent of the trajectories is concerned, Fig. 2 demonstrates that a number of them extend all along the whole rake probe. This underlines the fact that the dipoles can extend radially across the SOL over more than 3 cm.

It should be noted that the amplitude of the dipoles, defined as the difference between the maxima of hills and valleys, is proportional to the fluctuating radial velocity. It is shown in Fig. 4 as a function of radius. The fluctuating radial velocity created by the radially elongated dipoles remains almost constant from 55 mm up to 80 mm, where a sharp

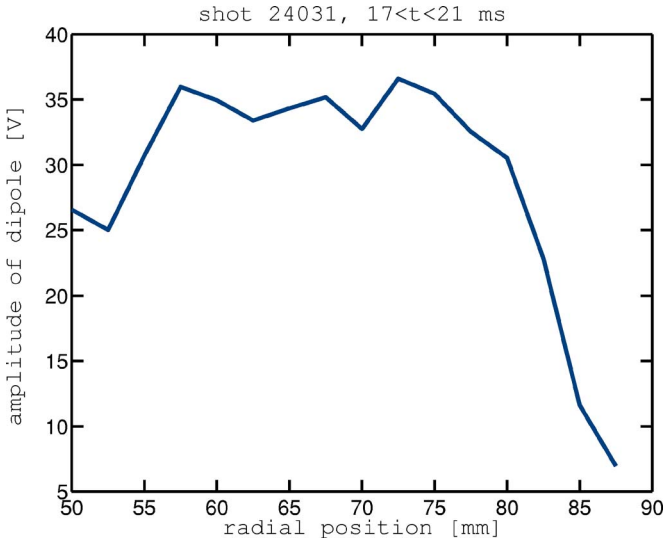

FIG. 4. Amplitude of dipoles as a function of radius.

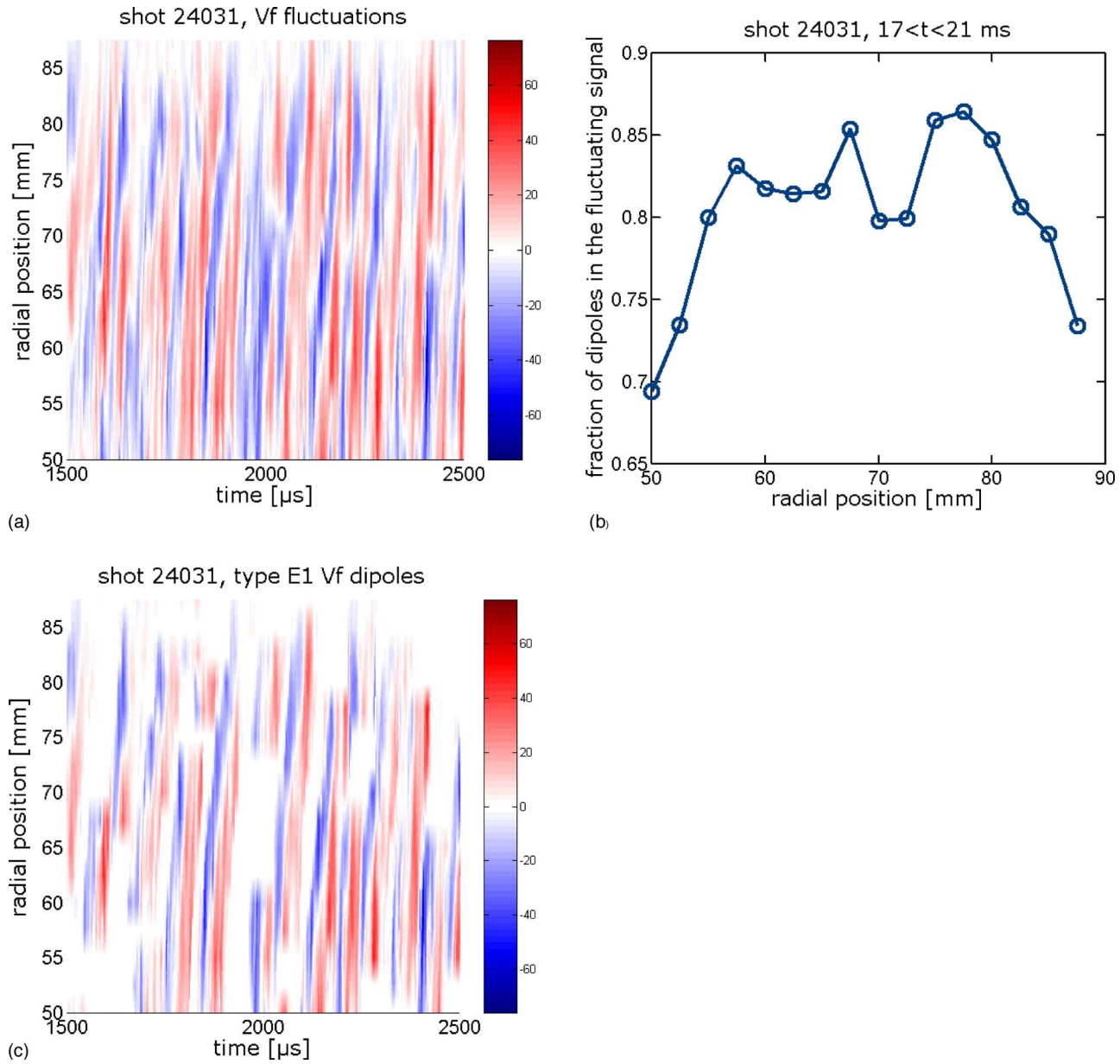

FIG. 5. (a) Top left, Vf fluctuations as a function of time on the rake. (b) Bottom left, reconstructed time signal with only dipoles E1. (c) Right, fraction of dipoles in total fluctuating signal as a function of radial position, averaged over time.

drop is observed. This indicates that the density bursts maintain their radial velocity over more than 2 cm, i.e., over most of the radial extent of the dipoles.

C. Fraction of dipoles in the fluctuating signal

The identification of all the dipoles of the type E1 on the rake probe allows us to reconstruct the signal corresponding to the dipoles only. Such a reconstruction is presented in Fig. 5. Figure 5(a) shows the 2D plot of raw potential fluctuations on the tips of the rake probe as a function of time, while in Fig. 5(b) only the fluctuations identified as dipoles similar to E1 (at least correlated to E1 with 60%) are plotted. All the rest of the signals have been set to zero. It is possible from these two figures to determine the fraction of type E1 dipoles in the total signal. To do this, the ratio

$$F(r) = \sqrt{\frac{\sum \delta V_d^2(r)}{\sum \delta V^2(r)}} \tag{2}$$

is calculated at every radial position r, where δV_d stands for the reconstructed signal from the dipoles and δV denotes the total potential fluctuations signal.

The result is plotted in Fig. 5(c), where it is seen that the potential dipoles of the type E1 contribute very significantly to the total signal, since the reconstructed signal corresponds to at least 70% of the total signal near the LCFS and this fraction grows up to 85% at 80 mm, where it starts to drop. This demonstrates that E1 is not a rare event but an essential component of the signal and that dipoles exist also in the vicinity of the LCFS.

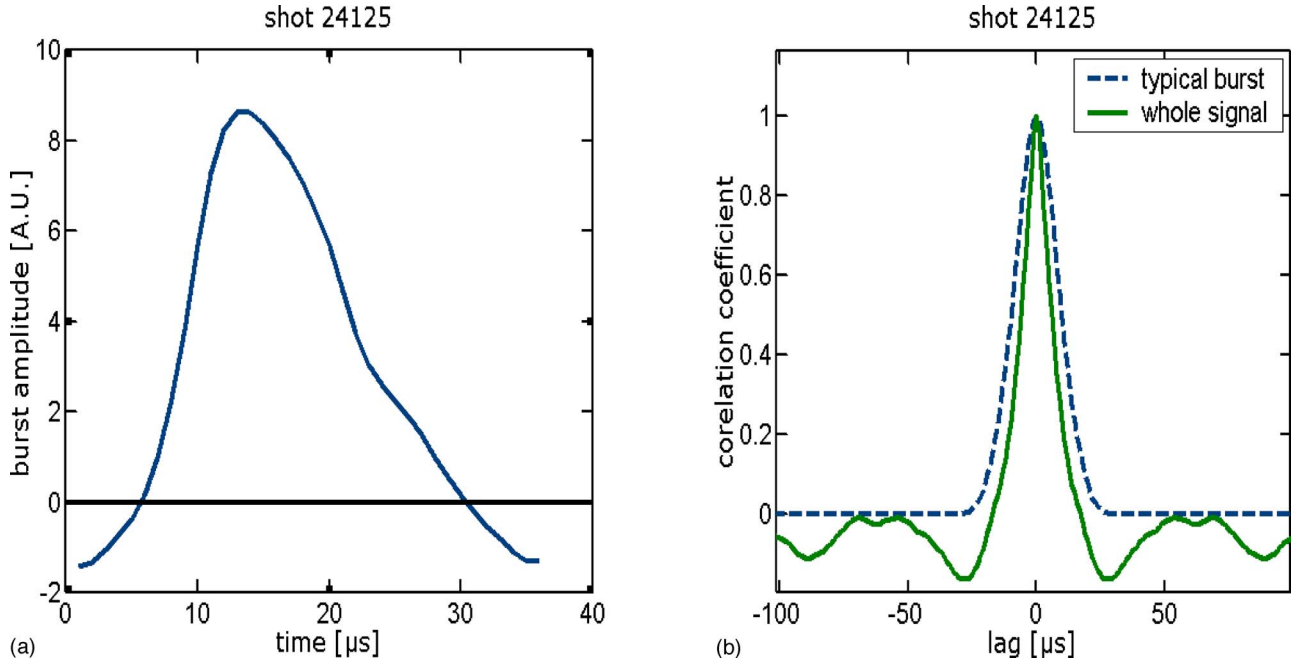

FIG. 6. (Left) Density burst measured on a probe of the rake in the SOL. Reference signal E2 for the trajectory analysis. (Right) Comparison of autocorrelation function of typical burst E2 with autocorrelation function of the whole signal.

V. DENSITY FLUCTUATIONS

A. Burst propagation in the SOL

The typical density event in the SOL of CASTOR is a burst of duration 30 μs. It is asymmetric, with a fast rising front and a slowly decaying tail, and it has a similar shape to what is observed in other machines.[15] It is plotted in Fig. 6(a) and is labeled as the typical event E2 in the following analysis. Its duration is about half of the duration of a potential dipole. Figure 6(b) compares the autocorrelation function of density fluctuations with that of burst E2. The small oscillation of the ACF of the total signal comes from the stationarization of the signal. The signal is composed of positive density bursts superposed on a positive background density, but to calculate the ACF, it is necessary to subtract the mean value, and the foot of the bursts becomes negative yielding the negative component of the ACF.

The result of the trajectory analysis is shown in Fig. 7 for a threshold value of $C(t)=0.8$. As in the case of potential fluctuations, the bursts are found to extend in the radial direction over a large fraction of the rake probe and sometimes all along it (3.75 cm).

This result is indicative of a long-range type of transport.

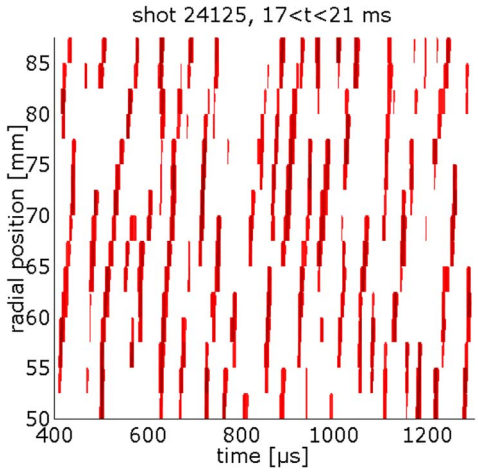

FIG. 7. Trajectories of density bursts type E2, along the rake probe in the SOL of CASTOR.

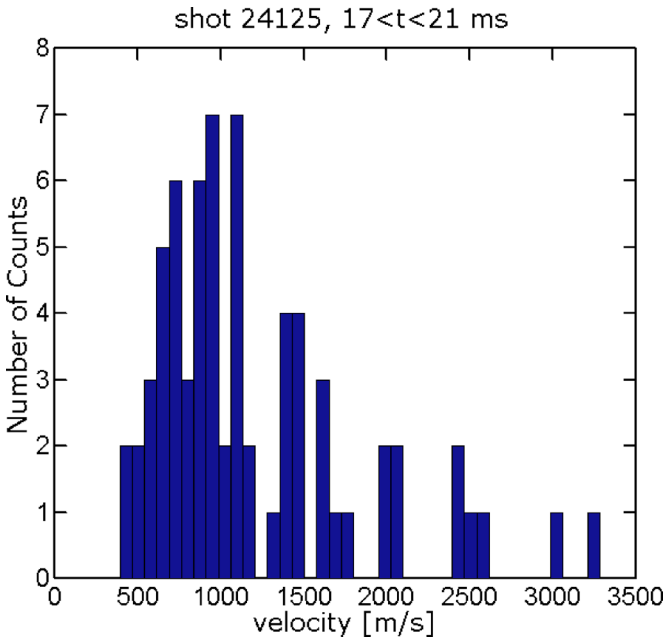

FIG. 8. Histogram of apparent radial velocities of bursts of type E2 in the SOL.

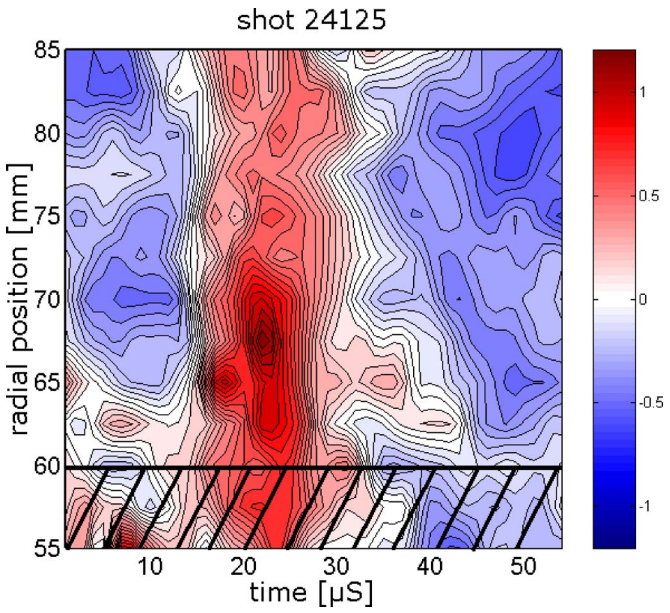

FIG. 9. Propagation of one burst of type E2, along the rake probe in the SOL. The shaded region corresponds to the shearing region.

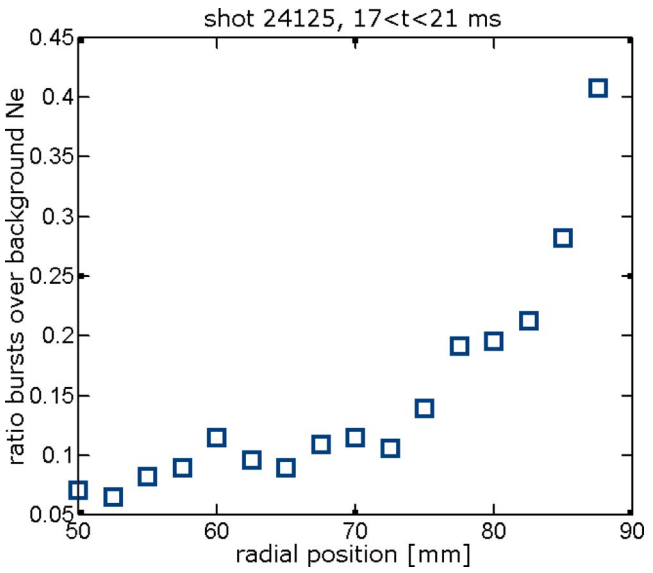

FIG. 10. Percentage of bursts relative to time averaged local density as a function of radius inside the SOL.

It is possible to get some statistics about the trajectories plotted in Fig. 7. The apparent radial velocities calculated for trajectories, which cover at least four probes, have been measured from the slope of the trajectories in Fig. 7. Their histogram is plotted in Fig. 8.

The most probable velocity is between 900 and 1000 m/s but the mean velocity is around 1300 m/s due to the existence of a tail of higher velocities. The standard deviation of the velocities is in this case $\sigma\ (v_{\mathrm{burst}})=1000$ m/s. The relative dispersion of the apparent velocities is $\sigma\ (v_{\mathrm{burst}})/\langle v_{\mathrm{burst}}\rangle=77\%$. This value must be compared with those obtained for the velocities of the potential dipoles $\sigma\ (v_{\mathrm{dipole}})/\langle v_{\mathrm{dipole}}\rangle=43\%$. It shows that the apparent radial velocities of the bursts are much more fluctuating than those of the potential dipoles. The dispersion of these velocities indicates that at least one of the components of the apparent radial velocity (with the poloidal and radial components) is turbulent. The result of Fig. 8 is in contrast with that obtained for the potential dipoles, whose apparent radial velocities have less dispersion but also a lower mean value. It suggests that potential and density fluctuations in CASTOR do not propagate with the same radial velocity, as will be discussed in more detail later.

It is possible to select one trajectory of the density bursts and plot it in its moving frame at every radial position. To do this, one burst is chosen and the maximum of $C(t)$ corresponding to this burst is found at each radial position. The signal in the corresponding time window is then plotted with the time shift removed. Thus we correct from the apparent radial velocity. The result is shown in Fig. 9 for a burst propagating within the SOL. Figure 9 is a typical one and is representative of most of the bursts that have been studied. The intensity of the burst is maximum up to 1–1.5 cm from the LCFS. The region with maximum intensity corresponds most probably to the region where the burst is created. A decrease of burst intensity by a factor of 2 is observed at 85 mm.

This observation that the burst intensity decays along the radius can be interpreted in the following way. The density bursts are understood as poloidally and radially localized structures that are extending all along the field lines. It is demonstrated in Ref. 10 that both density and potential fluctuations are correlated over several toroidal turns in CASTOR along the field lines with no measurable delay ($<1\ \mu$s). In the SOL, the density burst is a filament connecting both sides of the poloidal limiter that moves radially. The decrease of the burst intensity at large radii may be due to the parallel loss of particles to both sides of the limiter. The parallel loss of the density is driven by the sheath condition at the limiter where the velocity is the ion acoustic speed.

In order to observe these bursts far in the SOL, the radial transit time of the bursts across the SOL must be comparable to the parallel one. The parallel transit time is about $t_{\parallel}=L_{\parallel}/V_{\parallel}=300\ \mu$s, where $v_{\parallel}$ is the ion acoustic speed $v_{\parallel}=3\times 10^4$ m/s, and $L_{\parallel}=10$ m is a typical parallel connection length in CASTOR. The perpendicular transit time of the burst, $t_{\perp}=L_{\perp}/V_{\perp}$ (where $L_{\perp}=3$ cm is the radial extension of the burst on the rake probe), should be of the same order as $t_{\parallel}$ so that the radial velocity of the burst should be at least of the order of 100 m/s, which is much lower than the apparent mean radial velocity that is being measured.

B. Fraction of bursts relative to mean density

An important property of the bursts is that their density does not decrease radially as fast as the time averaged density. This is shown in Fig. 10, where the ratio

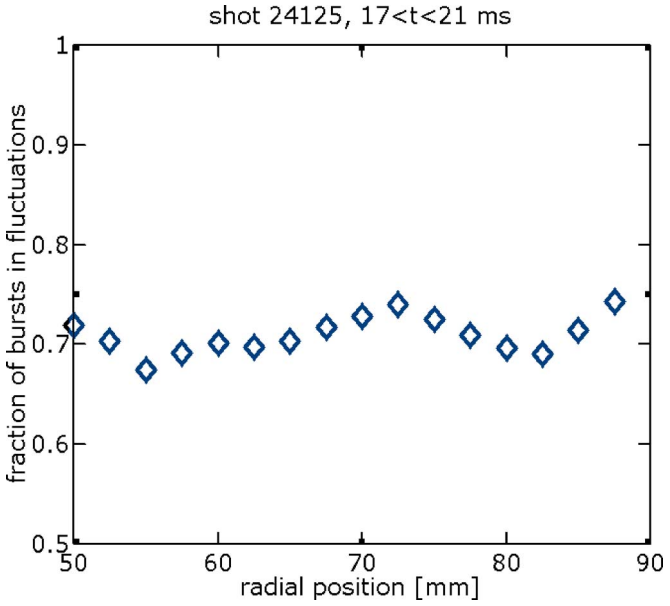

FIG. 11. Percentage of bursts type E2 in the total fluctuating signal as a function of radius in the SOL averaged over time.

$$F2(r) = \frac{\sqrt{\langle \delta N_d(r) \rangle^2}}{\langle N(r) \rangle} \tag{3}$$

is calculated as a function of the radius. In this expression, $\delta N_d(r)$ stands for the reconstructed signal with only the bursts, $\langle N(r) \rangle$ being the time average density at position r. Figure 10 shows that the fraction of bursts relative to the mean density increases strongly with the radius from about 70 mm. The fact that the ratio F2 is not constant along the radius indicates that the density bursts are not produced locally at every radial position but that they are formed at a particular radial position, probably in the region where the ratio is about constant <70 mm. It should be noted that this flat region corresponds roughly to the region where the burst intensity is maximum, see Fig. 9. The bursts propagate radially over the background density from that place toward the wall with a different velocity than the background density. This is an indication that the bursts do not merge so easily with the background density. All these results are in general agreement with the ones found in the literature.

C. Fraction of bursts in the fluctuating signal

The fraction of bursts similar to E2 in the total fluctuating signal has been calculated as a function of the radius using Eq. (2). The result is plotted in Fig. 11. It is found that this fraction remains almost constant along the radius and is around 70%. This indicates that bursts of the type E2 represent a substantial part of the signal at almost all radii including those close to the LCFS.

In contrast to other studies,[2] the bursts are not selected by a threshold method. In our case, the temporal bursts are selected according to their shape and duration, independently from their amplitude. This relative independence of the fraction of bursts with the radius can be confirmed by calculating the skewness of the signals. The skewness is a good indicator of the presence of bursts or spikes.

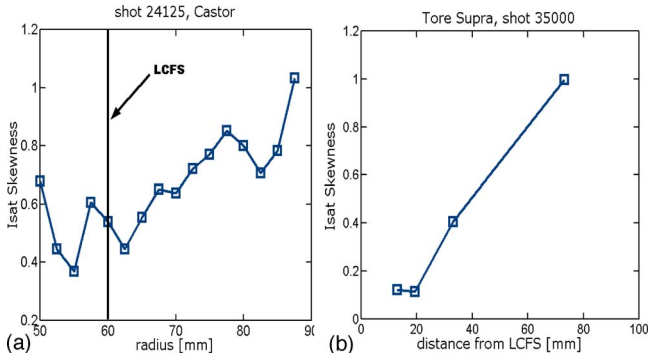

FIG. 12. (Left) Skewness of density fluctuations as a function of radius in the SOL of CASTOR. (Right) Skewness of density fluctuations as a function of radial distance from LCFS in the SOL of Tore Supra (R=2.34 m, a=0.72 m, Ip=1 MA).

The radial profile of skewness shown in Fig. 12(a) demonstrates that the skewness in the SOL increases toward the wall and is already high enough near the LCFS. This is different from the situation encountered in larger machines, e.g., TORE Supra [J. Jacquinot, Nucl. Fusion **43**, 1583 (2003)] [Fig. 12(b)], where a small skewness is measured in the vicinity of the LCFS on the SOL side for standard conditions.

VI. COMPARISON OF POLOIDAL VELOCITIES OF POTENTIAL AND DENSITY FLUCTUATIONS

In order to compare the poloidal velocities of potential and density fluctuations, it is necessary to measure them simultaneously in the same discharge. To this purpose, a poloidal ring of 124 probes covering the whole poloidal perimeter is inserted in the machine. A quadrant of the poloidal ring consisting of 32 probes separated by 3 mm is used for this measurement. As the probes measure alternately the ion saturation current and the floating potential, two subsequent probes in the same mode of operation are separated by 6 mm. The probes are located inside the SOL at a radial distance of several mm from the LCFS.

To measure the poloidal velocities of the fluctuations, the following procedure is applied: the signal of a reference probe of the poloidal ring is cross-correlated with the neighboring probes yielding several correlation functions. Only the cross-correlation functions that have a maximum larger than 0.3 are retained and the time shifts of the maxima relative to the reference probe are plotted versus the poloidal distance. This procedure is repeated for all the probes and the data points are accumulated on the same graph. To calculate the average poloidal velocity of the fluctuations along the ring, the data are fitted by a straight line by a least mean square fit. The poloidal velocity is then deduced from its slope. Figure 13 shows the result obtained for a time window of 3 ms during the flat top phase of the discharge. It is seen that the mean poloidal velocity of both potential and density fluctuations is equal to 1400 m/s. The velocity measured by each probe is also plotted in Fig. 13. It shows that for this

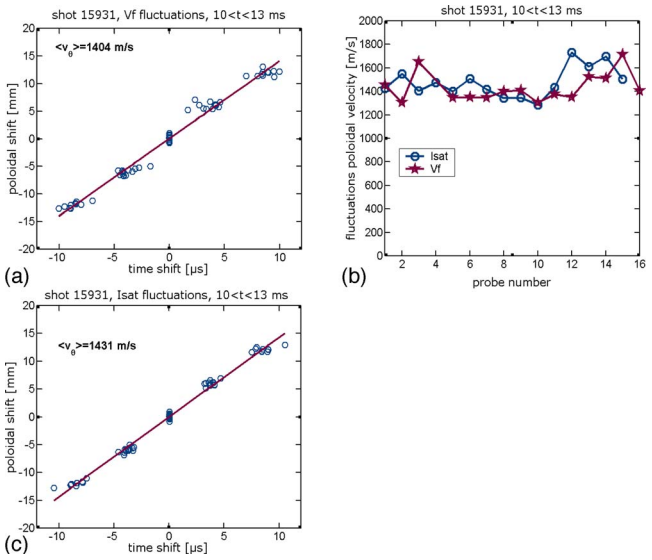

FIG. 13. (a) Top left, mean poloidal velocity of potential fluctuations on a segment of 90° of the poloidal ring. Also plotted is the least mean square fit. (b) Bottom left, same with density fluctuations. (c) Right, local mean poloidal velocity as a function of probe number along the 90° segment.

shot, the poloidal velocity is very uniform along this quadrant of the poloidal ring. This indicates that all the probes are radially located at about the same distance from the LCFS. Although the measured velocity is obtained from the whole fluctuation data, it certainly characterizes the behavior of the potential dipoles and density bursts that represent about 70% of the total signal, as it was shown in previous sections.

We conclude from these measurements that potential and density fluctuations are rotating poloidally with the same velocity. However, the apparent radial velocity of density bursts has been found to be much larger than that of the potential dipoles, as shown in Secs. IV B and V A. This cannot be attributed to the difference in their poloidal velocities. Consequently, the difference is attributed to different radial velocities. The radial velocity of the bursts is much larger than that of the dipoles.

VII. DISCUSSION

The analysis of the data yields the following picture of the turbulent transport in the SOL of the CASTOR tokamak. The potential dipoles are observed to be radially elongated structures, rotating poloidally, and they are expected (by reference to other measurements[11,12]) to be inclined in the (r,θ) plane.

The density bursts are seen to be created in the vicinity of the LCFS. They rotate poloidally with the same velocity as the potential fluctuations and propagate radially over a few centimeters without breaking up and with little modification in their shape. Their radial velocity is higher than that of the potential dipoles, indicating that they are streaming radially along the dipoles in the region, where the poloidal field of the dipole is maximum, without affecting them. This shows that density bursts and the potential dipoles are rather decoupled.

The physical picture derived above can be compared directly to the results of fluid codes such as the Tokam code[16,17] that models an interchange turbulence in the SOL of tokamaks. The interchange instability[18–20] is considered a good candidate to explain the turbulence in the SOL of fusion devices, although some other instabilities are also possible drives.[21] The Tokam code is 2D but it is believed to include most of the essential features of the SOL turbulence. The turbulence modeled by this code has two limiting states that correspond to different plasma edge conditions.

The first limiting state corresponds to a long parallel connection length and/or low collisionality of the SOL. This situation is, in general, more probable for large devices. In that case, the picture that emerges is similar to that of "blobs."[22] There is strong coupling between density and potential fluctuations, meaning that the density burst propagates with its own internal polarization so that the radial velocities of potential and density fluctuations are expected to be comparable. The large blobs are found to break up during their propagation so the radial correlation length is short.

The second limiting case corresponds to short connection lengths and/or high collisionality. In this case, the high collisionality refers to collisions with neutrals involving charge exchange that is a very efficient process for the loss of momentum. This high collisionality or equivalently the resulting viscosity leads to the formation of streamers or finger-like radially elongated potential structures. In this case, the density is decoupled from the potential meaning so that the internal polarization of the density burst is much weaker than the surrounding background potential field. Hence, the density burst can move radially without much affecting the potential turbulent field.

It is clear that the data of CASTOR are only compatible with the second case. For CASTOR, the parallel connection length is extended over several toroidal turns[23] in the SOL so that it is of the order of about 10 m and comparable to the one obtained in larger machines. On the other side, the fraction of neutrals at the edge of CASTOR seems sufficient to produce a high viscosity. A lower estimate of the neutral density put them at 10^{17} m^{-3} with a mean free path of the order of the plasma radius. This means that the neutral density is several percent of the plasma density in the SOL of CASTOR and this is in the range needed by the TOKAM code to produce a turbulence dominated by streamer-like features and where the density is decoupled from the potential field.

VIII. CONCLUSION

In this paper, radially and poloidally resolved probe measurements allow us to describe the turbulent transport in the SOL. This transport is found to be long range, with potential and density structures elongated over several cm in the radial direction. Both density and potential rotate poloidally at the same velocity, but density bursts propagate faster than the potential dipoles in the radial direction. This indicates that density bursts and potential dipoles are decorrelated and that density bursts are streaming along the potential structures without affecting them. This picture of the turbu-

lent transport is compatible with that described by an interchange fluid code in the limiting state where the feedback of zonal flows on the turbulence is negligible. Finally, this indicates that the viscosity at the edge of CASTOR is probably dominated by charge exchange with neutrals.

ACKNOWLEDGMENTS

Some data from Tore Supra were provided courtesy of I. Nanobashvili and J. Gunn.

[1] G. Y. Antar, S. I. Krasheninnikov, P. Devynck, R. P. Doerner, E. M. Hollmann, J. A. Boedo, S. C. Luckhardt, and R. W. Conn, Phys. Rev. Lett. **87**, 065001 (2001).
[2] G. Y. Antar, P. Devynck, X. Garbet, and S. C. Luckhardt, Phys. Plasmas **8**, 1612 (2001).
[3] J. A. Boedo, D. Rudakov, R. Moyer, S. Krasheninnikov, D. Whyte, G. McKee, G. Tynan, M. Schaffer, P. Stangeby, P. West, S. Allen, T. Evans, R. Fonck, E. Hollmann, A. Leonard, A. Mahdavi, G. Porter, M. Tillack, and G. Antar, Phys. Plasmas **8**, 4826 (2001).
[4] J. A. Boedo, D. L. Rudakov, R. A. Moyer, G. R. McKee, R. J. Colchin, M. J. Schaffer, P. G. Stangeby, W. P. West, S. L. Allen, T. E. Evans, R. J. Fonck, E. M. Hollmann, S. Krasheninnikov, A. W. Leonard, W. Nevins, M. A. Mahdavi, G. D. Porter, G. R. Tynan, D. G. Whyte, and X. Xu, Phys. Plasmas **10**, 2863 (2003).
[5] S. J. Zweben, D. P. Stotler, J. L. Terry, B. LaBombard, M. Greenwald, M. Muterspaugh, C. S. Pitcher, K. Hallatschek, R. J. Maqueda, B. Rogers, J. L. Lowrance, V. J. Mastrocola, G. F. Renda, and Alcator C-Mod Group, Phys. Plasmas **9**, 1981 (2002).
[6] J. L. Terry, S. J. Zweben, K. Hallatschek, B. LaBombard, R. J. Maqueda, B. Bai, C. J. Boswell, M. Greenwald, D. Kopon, W. M. Nevins, C. S. Pitcher, B. N. Rogers, D. P. Stotler, and X. Q. Xu, Phys. Plasmas **10**, 1739 (2003).
[7] G. Van Oost, J. Adámek, V. Antoni, P. Balan, J. A. Boedo, P. Devynck, I. Ďuran, J. P. Gunn, M. Hron, C. Ionita, S. Jachmich, G. S. Kirnev, E. Martines, A. Melnikov, R. Schrittwieser, C. Silva, J. Stöckel, M. Tendler, C. Varandas, M. Van Schoor, V. Vershkov, and R. R. Weynants, Plasma Phys. Controlled Fusion **45**, 621 (2003).
[8] P. Devynck, J. Stockel, J. Adamek, I. Duran, M. Hron, and G. Van Oost, Czech. J. Phys. **53**, 10853 (2003).
[9] M. Spolaore, J. Brotankova, P. Peleman, P. Devynck, H. Figueiredo, G. Kirnev, E. Martines, J. Stoeckel, G. Van Oost, J. Adamek, E. Dufkova, I. Duran, M. Hron, and V. Weintzel, Czech. J. Phys. (to be published).
[10] P. Devynck, G. Bonhomme, E. Martines, J. Stoeckel, G. Van Oost, I. Voitsekhovitch, J. Adamek, A. Azeroual, F. Doveil, I. Duran, E. Gravier, J. Gunn, and M. Hron, Plasma Phys. Controlled Fusion **47**, 269 (2005).
[11] M. Endler, H. Niedermeyer, L. Giannone, E. Holzauer, A. Rudyj, G. Theimer, N. Tsois, and the ASDEX Team, Nucl. Fusion **35**, 1307 (1995).
[12] J. Bleuel, M. Endler, H. Niedermeyer, M. Schubert, H. Thomsen, and the W7-AS Team, New J. Phys. **4**, 38 (2002).
[13] M. Spolaore, V. Antoni, E. Spada, H. Bergsåker, R. Cavazzana, J. R. Drake, E. Martines, G. Regnoli, G. Serianni, and N. Vianello, Phys. Rev. Lett. **93**, 215003 (2004).
[14] B. K. Joseph, R. Jha, P. K. Kaw, S. K. Mattoo, C. V. S. Rao, Y. C. Saxena, and the Aditya Team, Phys. Plasmas **4**, 4292 (1997).
[15] G. Y. Antar, G. Counsell, Y. Yu, B. Labombard, and P. Devynck, Contrib. Plasma Phys. **44**, 217 (2004).
[16] Y. Sarazin, Ph. Ghendrih, G. Attuel, C. Clement, X. Garbet, V. Grandgirard, M. Ottaviani, S. Benkadda, P. Beyer, N. Bian, and C. Figarella, J. Nucl. Mater. **313-316**, 796 (2003).
[17] Y. Sarazin and Ph. Ghendrih, Phys. Plasmas **5**, 4214 (1998).
[18] A. V. Nedospasov, Sov. J. Plasma Phys. **15**, 659 (1989).
[19] X. Garbet, L. Laurent, J.-P. Roubin, and A. Samain, Nucl. Fusion **31**, 967 (1991).
[20] S. Benkadda, X. Garbet, and A. Verga, Contrib. Plasma Phys. **34**, 247 (1994).
[21] S. I. Krasheninnikov, A. I. Smolyakov, and T. K. Soboleva, Phys. Plasmas **12**, 072502 (2005).
[22] S. I. Krasheninnikov, Phys. Lett. A **283**, 368 (2001).
[23] J. Stöckel, P. Devynck, J. Gunn, E. Martines, G. Bonhomme, I. Voitsekhovitch, G. Van Oost, M. Hron, I. Duran, P. Stejskal, J. Adamek, V. Weinzettl, and F. Zacek, Plasma Phys. Controlled Fusion **47**, 635 (2005).